Available online at www.sciencedirect.com
ScienceDirect
Mendeleev Commun., 2013, **23**, 361–363
Mendeleev Communications

Crystallization mechanism of basalt glass fibers in air

Mikhail S. Manylov,* Sergey I. Gutnikov, Konstantin V. Pokholok, Bogdan I. Lazoryak and Yakov V. Lipatov

Department of Chemistry, M. V. Lomonosov Moscow State University, 119991 Moscow, Russian Federation. Fax: +7 495 939 3316; e-mail: manylov.msu@gmail.com, gutnikov@gmail.com

DOI: 10.1016/j.mencom.2013.11.021

As found by differential thermal analysis, X-ray diffraction and Mössbauer spectroscopy, the heat treatment of basalt glass fibers in air leads to complete iron oxidation and the bulk growth of superparamagnetic magnesioferrite particles which act as nucleation sites for pyroxene crystallization.

Basalt glasses belong to the iron-rich Na_2O–K_2O–MgO–CaO–FeO–Fe_2O_3–SiO_2–Al_2O_3 aluminosilicate system. Many types of materials are manufactured on this basis, *e.g.*, rock (mineral or stone) wool,[1] glass-ceramics and glass fibers.[2,3] The crystallization of basalt glasses determines both the fiber production process confines (many yarn breaks and narrow production temperature range) and the operating temperature of materials based on basalt glasses.

Crystallization in basalt glasses was studied in detail.[4,5] It was found that the crystallization begins with spontaneous magnetite (Fe_3O_4) formation, which is favored by the initial liquid-liquid separation; the magnetite crystals become nucleation sites for the precipitation of a major phase with pyroxene structure. The kinetics of crystallization in bulk glasses was interpreted as a three-dimensional diffusion-controlled pyroxene-like formation on a fixed number of nuclei.

Thus, the iron cations play a key role in the crystallization of basalt glasses, however, basalt continuous fibers (BCFs) crystallization mechanism is still not defined precisely.[6,7]

In this work, basalt powder was heated in a platinum crucible in a high temperature furnace at a heating rate of 300 K h^{-1} up to 1473 K and at 50 K h^{-1} in a temperature range of 1473–1873 K; then, it was homogenized at 1873 K for 20 h. After that the melted basalt glass was rapidly quenched in water. As determined by X-ray fluorescence analysis, the chemical composition of the glass obtained was the following (wt%): (56.1±0.6) SiO_2, (15.5±0.4) Al_2O_3, (9.9±0.2) Σ(FeO + Fe_2O_3), (8.7±0.3) CaO, (4.0±0.1) MgO, (2.4±0.1) K_2O, (2.3±0.2) Na_2O and (1.1±0.1) TiO_2. The BCFs were produced by pulling from glass melt on a laboratory scale system[8] at 1723 K. The fiber diameter was controlled by varying the reel rotation rate. We used fibers 10–11 μm in diameter.

To characterize the glass transition and crystallization processes in BCFs, simultaneous thermal analyses (DSC and TG) were carried out in air.† Figure 1 shows the DSC output and mass change as a function of temperature. An increase of ~0.3 wt% on the TG curve in a temperature range of 900–1100 K follows from the oxidation of ferrous cations to ferric ones.[5,9] The DSC trace shows the glass transition (T_g = 980 K) and three exothermal peaks at the temperatures T_{p1} = 1105 K, T_{p2} = 1219 K and T_{p3} = 1387 K, which correspond to crystallization processes in BCFs.

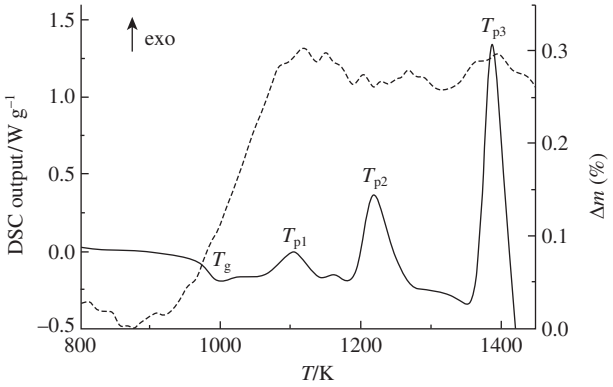

Figure 1 DSC output (solid curve) and mass change (dashed curve) of BCFs in air at a heating rate of 20 K min^{-1}. T_g is the glass transition temperature; T_{p1}, T_{p2} and T_{p3} are the exothermal peak temperatures.

Table 1 DSC measurements of BCFs (±2 K).

Heating rate/K min^{-1}	T_g	T_{p1}	Δw_{p1}	T_{p2}	T_{p3}
0[a]	969	1048	—	1175	1365
10	975	1075	43	1198	1374
20	980	1105	50	1219	1387
30	986	1134	57	1245	1395

[a]The values were estimated by the linear extrapolation of peak temperatures measured at heating rates of 10, 20 and 30 K min^{-1} to a zero heating rate.

For studying the kinetics of crystallization in BCFs, the DSC experiment was performed at heating rates of 10, 20 and 30 K min^{-1} (Table 1). The activation energy and the frequency factor of the nucleating phase crystallization (the first exothermal peak) were determined by Kissinger's method[10] based on the dependence of the crystallization peak temperature on the heating rate:

$$\ln(\beta/T_p^2) = \ln(A_c R/E_c) - E_c/RT_p, \quad (1)$$

where β is the heating rate, T_p is the crystallization peak temperature, A_c is the frequency factor of crystallization, E_c is the activation energy of crystallization and R is the gas constant.

The Avrami parameter for nucleation was calculated for each heating rate using the Augis–Bennett equation[11]

$$n = (2.5/\Delta w)(RT_p^2/E_c), \quad (2)$$

† Thermal analysis was carried out using a NETZSCH STA 449C Jupiter simultaneous thermal analyzer. Differential scanning calorimetric (DSC) and thermogravimetric (TG) signals were simultaneously recorded in a temperature range from 298 to 1473 K at heating rates of 10, 20 and 30 K min^{-1} in air. The correction of DSC signals was performed by measuring a baseline with two empty platinum crucibles under the same conditions.

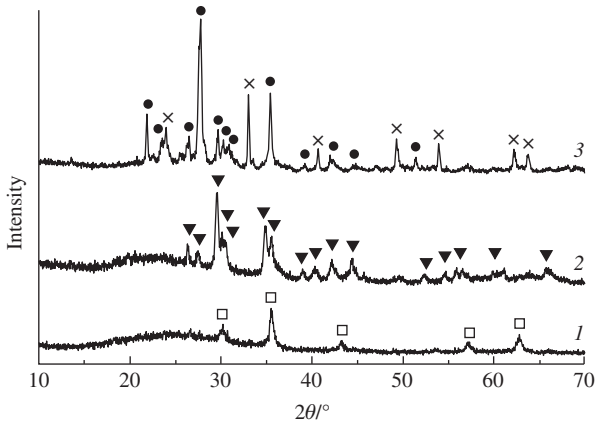

Figure 2 XRD patterns of the BCFs heat-treated at (*1*) 1048, (*2*) 1175 and (*3*) 1365 K for 24 h in air. The peaks were assigned to (□) maghemite, (▼) pyroxene, (×) hematite and (●) plagioclase.

where n is the Avrami parameter, Δw is the crystallization peak width at half maximum, and E_c is the activation energy of crystallization determined by Kissinger's method. Then, the obtained values of n were averaged.

The calculated activation energy, frequency factor and Avrami parameter of the nucleating phase crystallization are $E_c = (171\pm9)$ kJ mol^{-1}, $A_c = (3.8\pm0.2)\times10^7$ s^{-1} and $n = 3.0\pm0.3$, respectively. According to published data,[12] the estimated Avrami parameter indicates the bulk growth of nuclei in BCFs.

To study the crystallization under isothermal conditions, the BCFs samples were annealed at 1048, 1175 and 1365 K in a muffle furnace for 24 h. The temperatures were chosen based on the DSC results at a zero heating rate. The crystalline phases formed in annealed BCFs were identified by X-ray diffraction (XRD) analysis (Figure 2).‡

The BCFs were fully amorphous before heat treatment. The crystallization begins from the formation of a spinel phase at 1048 K, which was identified by XRD as magnesioferrite ($MgFe_2O_4$) [ICDD no. 73-2211]. The magnesioferrite particles act as nucleation sites for the crystallization of augite [$Ca(Fe,Mg)Si_2O_6$] [ICDD no. 24-201] at 1175 K. At 1365 K, anorthite ($CaAl_2Si_2O_8$) [ICDD no. 2-523] and hematite (Fe_2O_3) [ICDD no. 89-598] become dominant crystalline phases.

The redox state and local environment of iron in untreated and annealed BCFs were investigated by Mössbauer spectroscopy (Figure 3 and Table 2).§ The spectrum of the untreated BCFs [Figure 3(*a*)] was fitted with three doublets with isomer shifts of 1.02, 0.82 and 0.32 mm s^{-1}. The first two doublets correspond to ferrous ions and the third one, to ferric.[13] The Fe^{2+}/Fe^{3+} ratio is ~1/2. A very large line width (FWHM, Γ) is a consequence of the presence of a large number of distorted oxygen polyhedra with similar crystallographic parameters in fibers.

Heat treatment at 1048 K leads to the complete oxidation of iron to a ferric state and the formation of a spinel phase [Figure 3(*b*)].

‡ X-ray diffraction analysis was performed at room temperature on a Thermo ARL X'TRA powder diffractometer ($CuK_{\alpha1}$ radiation, λ = 1.54060 Å; $CuK_{\alpha2}$ radiation, λ = 1.54443 Å; intensity ratio $CuK_{\alpha1}/CuK_{\alpha2}$ = 0.51) with a Peltier-cooled solid state detector. XRD patterns were collected in the range 2θ = 10–70° with a step 0.02° and a scan rate of 1° min^{-1}. The crystalline phases were identified using the Crystallographica Search-Match software and the International Center for Diffraction Data (ICDD) database.

§ Mössbauer spectra were collected using a ^{57}Co single-line source embedded in Rh. Isomer shifts were referred to metallic α-Fe. All spectra were first collected on a large velocity scale between –10 and +10 mm s^{-1}. Spectra showed no indication of magnetic interaction, were re-collected on a smaller velocity scale between –4 and +4 mm s^{-1} to improve resolution. The spectra were fitted using the Univem MS software.

Table 2 Parameters of the Mössbauer spectra obtained at 298 K (δ is the isomer shift related to α-Fe, Δ is the quadrupole splitting, and Γ is the line width at half maximum).[a]

Samples	Components	δ	Δ	Γ	Area (%)[b]
Untreated BCFs	Fe^{2+}(doublet)-1	1.02	1.78	0.72	29
	Fe^{2+}(doublet)-2	0.82	2.93	0.46	6
	Fe^{3+}(doublet)-3	0.32	1.25	0.76	65
BCFs annealed at 1048 K	Fe^{3+}(doublet)-1	0.29	0.59	0.49	43
	Fe^{3+}(doublet)-2	0.34	1.01	0.65	52
	Fe^{3+}(doublet)-3	0.42	0.62	0.25	5

[a] ±0.03 mm s^{-1}. [b] ±5%.

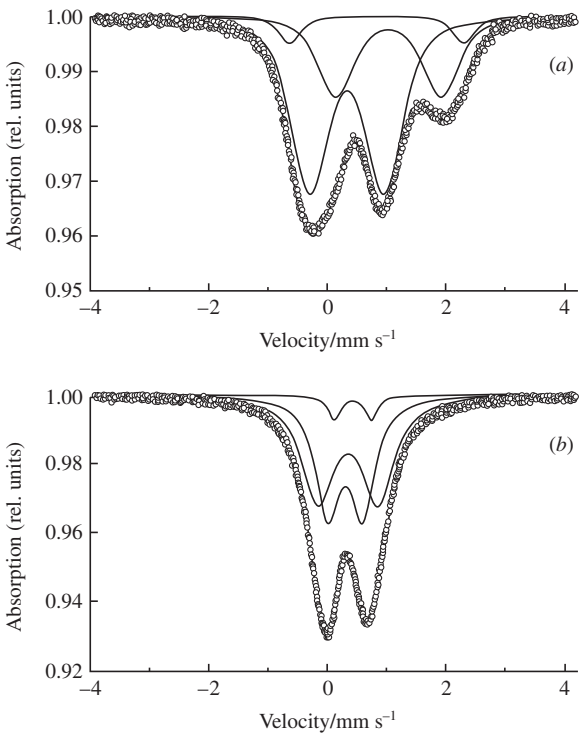

Figure 3 Mössbauer spectra collected at 298 K: (*a*) the untreated BCFs and (*b*) the BCFs annealed at 1048 K.

Doublets with isomer shifts of 0.34 and 0.42 mm s^{-1} were referred to ferric ions located in octahedral (^{VI}[Fe]) oxygen environments and a doublet with δ = 0.29 mm s^{-1} was attributed to ions in tetrahedral (^{IV}[Fe]) sites.[13] Magnesioferrite has an intermediate spinel structure represented by the formula $^{IV}[Mg_{1-x}Fe_x]$ $^{VI}[Mg_{x/2}Fe_{1-x/2}]_2O_4$.[14] The estimated ^{IV}[Fe]/^{VI}[Fe] ratio in the spinel phase is 0.75, which corresponds to x = 0.86.

Cooling the heat-treated sample down to a liquid nitrogen temperature (78 K) leads to the appearance of magnetic hyperfine splitting in the spectrum [Figure 4(*a*)]. This fact indicates the transition of a fraction of magnesioferrite particles in annealed BCFs to a magnetically ordered state, while about 30 mol% of them remain superparamagnetic.[15] Usually, the spectra of spinel-like materials (magnetite, maghemite *etc*.) above the Curie temperature contain a singlet rather than doublets.[16] The presence of superparamagnetic doublets in the spectra shown in Figures 3(*b*) and 4(*a*) indicates that a significant part of ferric ions is located in the region of the nanoparticle surface, and these ions are exposed to a nonzero electric field gradient due to distorted cubic symmetry.[17] The broadened sextet [Figure 4(*a*)] was fitted with an internal field distribution $P(H_{in})$ with a field range of 300–510 kOe and a step of 5 kOe [Figure 4(*b*)]. The fitting sextets have zero quadrupole splitting, and the isomer shift equals 0.42 mm s^{-1}. The maximum-probability hyperfine field and the half-width of

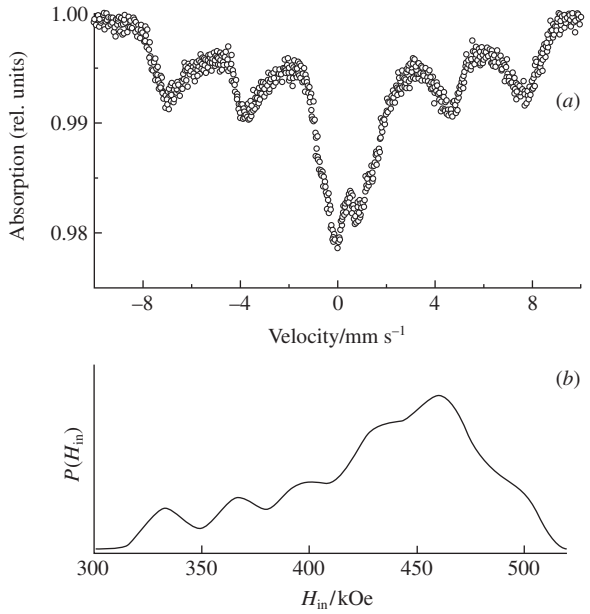

Figure 4 (*a*) Mössbauer spectrum (78 K) of the BCFs annealed at 1048 K and (*b*) the internal magnetic field distribution $P(H_{in})$.

the distribution are 465 and 80 kOe, respectively. The results correspond to poorly crystallized magnesioferrite with a wide particle-size distribution with an average value of 6 nm.[18]

The obtained results can be used for development of methods for inhibition of the basalt fiber crystallization.

This work was supported by the Russian Foundation for Basic Research (grant no. 12-03-31072-mol_a).

References

1 M. Moesgaard, H. D. Pedersen, Y. Z. Yue and E. R. Nielsen, *J. Non-Cryst. Solids*, 2007, **353**, 1101.
2 Ya. V. Lipatov, S. I. Gutnikov, M. S. Manylov and B. I. Lazoryak, *Inorg. Mater.*, 2012, **48**, 751 (*Neorg. Mater.*, 2012, **48**, 858).
3 S. I. Gutnikov, A. P. Malakho, B. I. Lazoryak and V. S. Loginov, *Russ. J. Inorg. Chem.*, 2009, **54**, 191 (*Zh. Neorg. Khim*., 2009, **54**, 223).
4 A. Karamanov and M. Pelino, *J. Non-Cryst. Solids*, 2001, **281**, 139.
5 A. Karamanov, P. Pisciella and M. Pelino, *J. Eur. Ceram. Soc.*, 2000, **20**, 2233.
6 E. A. Moiseev, S. I. Gutnikov, A. P. Malakho and B. I. Lazoryak, *Inorg. Mater*., 2008, **44**, 1026 (*Neorg. Mater*., 2008, **44**, 1148).
7 M. S. Manylov, S. I. Gutnikov, Ya. V. Lipatov, K. V. Pokholok, D. S. Filimonov and B. I. Lazoryak, *Fiz. Khim. Stekla*, 2012, **38**, 565 (in Russian).
8 S. I. Gutnikov, M. S. Manylov, Ya. V. Lipatov, B. I. Lazoryak and K. V. Pokholok, *J. Non-Cryst. Solids*, 2013, **368**, 45.
9 J. Rzechula and M. Grylicki, *Ceram. Int*., 1980, **6**, 39.
10 H. E. Kissinger, *Anal. Chem*., 1957, **29**, 1702.
11 J. A. Augis and J. E. Bennett, *J. Thermal Anal.*, 1978, **13**, 283.
12 S. Yilmaz, O. T. Özkan and V. Günay, *Ceram. Int.*, 1996, **22**, 477.
13 F. Menil, *J. Phys. Chem. Solids*, 1985, **46**, 763.
14 S. M. Antao, I. Hassan and J. B. Parise, *Am. Mineral.*, 2005, **90**, 219.
15 M. Siddique, E. Ahmed and N. M. Butt, *Physica B*, 2010, **405**, 3964.
16 J. M. Florez, J. Mazo-Zuluaga and J. Restrepo, *Hyperfine Interact.*, 2005, **161**, 161.
17 D. Satula, B. Kalska-Szostko, K. Szymanski, L. Dobrzynski and J. Kozubowski, *Acta Phys. Pol. A*, 2008, **114**, 1615.
18 Q. Chen, A. J. Rondinone, B. C. Chakoumakos and Z. J. Zhang, *J. Magn. Magn. Mater.*, 1999, **194**, 1.

Received: 11th April 2013; Com. 13/4102